RANS prediction of the aerodynamic losses in a linear turbine cascade with an upstream cavity and a purge flow

Fatih Uncu, Benjamin François, Raphaël Barrier, Nicolas Buffaz, Sébastien Le Guyader

RANS PREDICTION OF THE AERODYNAMIC LOSSES IN A LINEAR TURBINE CASCADE WITH AN UPSTREAM CAVITY AND A PURGE FLOW

F. Uncu[1] *- B. François*[2] *- R. Barrier*[2] *- N. Buffaz*[3] *- S. Le Guyader*[3]

[1] PhD candidate at Safran Helicopter Engines / ONERA, fatih.uncu@onera.fr
[2] Research engineer at ONERA, CFD Turbomachinery Team, 92190 Meudon France
[3] Engineer at Safran Helicopter Engines, 64511 Bordes France

ABSTRACT

In a turbomachine, gaps separate stator and rotor disks. For turbines, often a purge flow is blown through these gaps in order to seal and avoid hot air to penetrate deep in the turbine disk components and over-solicit them. The interaction of this purge flow with the main flow creates and amplifies vortex structures, responsible for aerodynamic losses. Accurately predicting these losses remain a challenge with RANS approach for engine manufacturers that wish to design an efficient cavity geometry minimising the losses while ensuring the sealing. The Boussinesq approximation fails in such flows where a high turbulence level and anisotropy are present. Therefore, in RANS, the use of two-equation linear eddy-viscosity turbulence models is questionable. The present work assesses a second order Reynolds Stress Model (RSM), as well as two eddy-viscosity models, in a linear turbine cascade with an upstream cavity from which a purge flow emanates. The specificity of this cascade is the high external turbulence intensity (6%), which is all the more challenging in a RANS approach. Different purge mass flows and three configurations are evaluated: two with different cavities and one without any. The RANS simulations are compared to experimental data. All the RANS models show the same trends: the presence of a cavity induces additional pressure losses; increasing the purge mass flow helps to seal the cavity entry but nourishes the passage vortex and thus leads to additional losses. The RSM simulation shows the best agreement with the measurements and is the only one that predicts the loss evolution when the cavity chute geometry changes.

KEYWORDS

Linear Cascade, Low-Pressure Turbine, Cavity Flow, RANS Turbulence Modelling

NOMENCLATURE AND SUBSCRIPTS

C_x	Axial chord of the linear cascade	
LE / TE	Leading edge / Trailing edge of the blade	
k (TKE)	Turbulent Kinetic Energy	
μ_t	Eddy viscosity	
P_i	Stagnation pressure	
P_s	Static pressure	
T_i	Stagnation temperature	
$C_p(x)$	Static pressure coefficient	$(P_{i,1}-P_s(x))/(P_{i,1}-P_{s,2})$
ζ	Stagnation pressure loss coefficient	$(P_{i,1}-P_{i,2})/(P_{i,2}-P_{s,2})$
θ	Normalised fluid temperature	$(T_i-T_{i,leakage})/(T_{i,\infty}-T_{i,leakage})$
S / Ω	Shear / Vorticity tensor	
$_1$	Subscript denoting a position at 1 C_x upstream of the leading edge	
$_2$	Subscript denoting a position at 1/4 C_x downstream of the trailing edge	

INTRODUCTION

A 50% drop in the purge mass flow could lead to a 0.5% increase in the efficiency of a two stage high-pressure turbine and to a 0.9% decrease in the specific fuel consumption [1]. Although less used in low-pressure turbines, it is essential to reduce purge flow and to improve cavity sealing to minimise interaction with mainstream flow. However, increasing the combustion chamber exit temperature in modern engines requires more purge flow. The interaction between cool purge flow and main flow creates a shear layer causing viscous losses. In addition, the flow angle is modified at the leading edge of the downstream blade, which disrupts the turbine work. Furthermore, main flow ingress can also occur; this is mainly because of disk pumping, vane/blade periodic pressure field and cavity chute seal geometry [1]. The first two mechanisms are also functions of the latter. Bailey and Owen [2] showed that disk pumping depends directly on the spacing between the two walls of the chute. A spacing smaller than the boundary layer thickness helps in reducing purge flow necessary for sealing. Complex geometries with overlaps between the two walls of the cavity help reduce the flow exchange between the cavity and the main channel, resulting in significant reductions in aerodynamic losses [3; 4].

The prediction of cavity flows and their impact on the pressure losses of the turbine must be taken into account in RANS simulations during the design stage. However, in regions of complex geometry that present multiple separations, reattachments and mixing process, like in the cavity sealing flows, RANS modelling may not predict accurate results [5]. The high turbulence production and important turbulence anisotropy in such non-equilibrium regions are still challenging for the classical eddy-viscosity turbulence models.

The main studies on cavity flows use the $k-\omega$ SST model with a Kato-Launder limiter ([6; 7]). Horwood *et al.* [8; 9] showed that RANS simulations well-predict the velocity field and sealing efficiency in the cavity. However, when the purge flow increases, the simulation under-predicts the ingress. RANS modelling produces too much eddy viscosity which stabilises vortex structures leading to a misprediction of the sealing. The level of ingress and egress also modifies the size of the passage vortex which is the source of pressure losses. These losses are mispredicted with RANS turbulence models in a simple turbine stage.

Izenson *et al.* [10] compare measurements with $k-\varepsilon$ and an RSM model based on Rotta's distribution term. The components of the Reynolds stress tensor calculated by the RSM model are anisotropic. The directional dependence of the velocity fluctuations is absent in a linear eddy-viscosity model. In highly rotational stress flow, where streamline curvature is high, the anisotropy is important, and in such an environment the RSM model provides predictions closer to the experiment. Furthermore, the measurements of Porreca *et al.* [11] at a stator/rotor interface show a difference of 45% between radial and streamwise component of fluctuations.

The present work proposes to assess RANS turbulence models in a turbine cascade with a high level of external turbulence. A hub cavity from which a purge flow emanates is present upstream of the blade leading edge. Different cavity geometries and purge mass flows are simulated. The aim is to assess the ability of RANS simulations in accurately predicting the pressure losses related to the cavity and understand the importance of turbulence modelling in such flows. A second order Reynolds Stress Model (SSG/LRR-ω [12]) as well as two eddy-viscosity models ($k-\omega$ SST [13] and $k-l$ [14]) are evaluated.

Firstly, the paper introduces the three simulated configurations. Then, the numerical setup and the meshes are presented. Finally, results with different turbulence models are discussed and compared to the measurements.

CONFIGURATIONS

Instrumentation

The simulated configuration is a linear cascade from the EU project MAGPI[1], which aimed to improve turbine cavity designs. It is composed of five stator blades. The hub and shroud are flat, and a cavity is present just before the leading edge at the hub. A turbulence grid located at seven axial chords (C_x) upstream imposes the turbulence intensity on the incoming flow. The rig test and measurement instrumentation are detailed by Schuler *et al.* [4] and summarised in Fig. 1.

A five-hole probe located at 1 C_x upstream of the leading edge of the blade (LE) measures the angle, stagnation temperature (with a thermocouple) and stagnation pressure. Measurements are also done at 1/4 C_x downstream of the trailing edge of the blade (TE). The static pressure is measured on the central blade at 6% channel height.

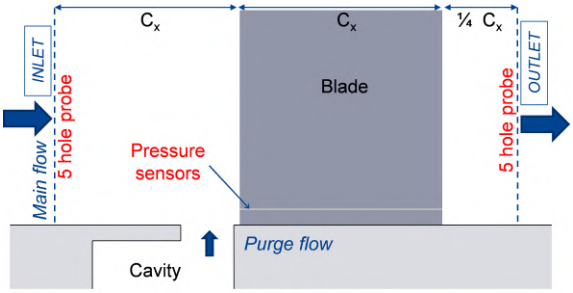

Figure 1: Rig instrumentation

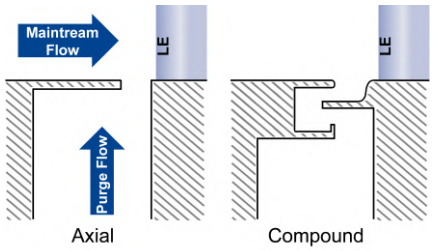

Figure 2: Simulated cavities

Cavity geometry

Three configurations are simulated: two with a cavity and one without any. The geometry of the *Axial* and *Compound* cavities are shown in Fig. 2. They are located at the same axial position (0.044 C_x upstream of the LE). The seal of the first one is orthogonal to the hub of the channel and has sharp edges; the latter is tangential and has a more complex geometry. The compound cavity outlet is not straight; the flow has to cross the fillet obstacle and bend for reaching the main channel. The chute of the cavity is the only geometrical difference between both configurations. The terms used in the following sections are defined in Fig. 3.

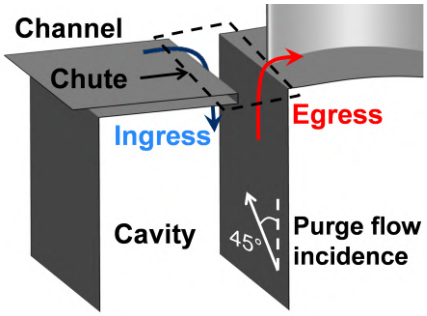

Figure 3: Definitions

NUMERICAL SIMULATIONS

The computational domain has been reduced to one blade considering that the flow is laterally periodic. The domain starts at 1 C_x upstream of the LE and ends at 1 C_x downstream of the TE. The experimental stagnation pressure $P_{i,1}$, stagnation temperature $T_{i,1}$ and flow angle are imposed at the inlet, and the exit pressure corresponds to the experimental wall static pressure. The purge mass flow is directly imposed at the cavity inlet so that it represents 0% (no purge flow), 0.5% and 1.0% of the channel mass flow. As in the experiment, the purge flow is injected with an angle of 45° in the stream-normal plane (Fig. 3) and is 30 K cooler than

[1]Main Annulus Gas Path Interactions : https://cordis.europa.eu/project/id/30874

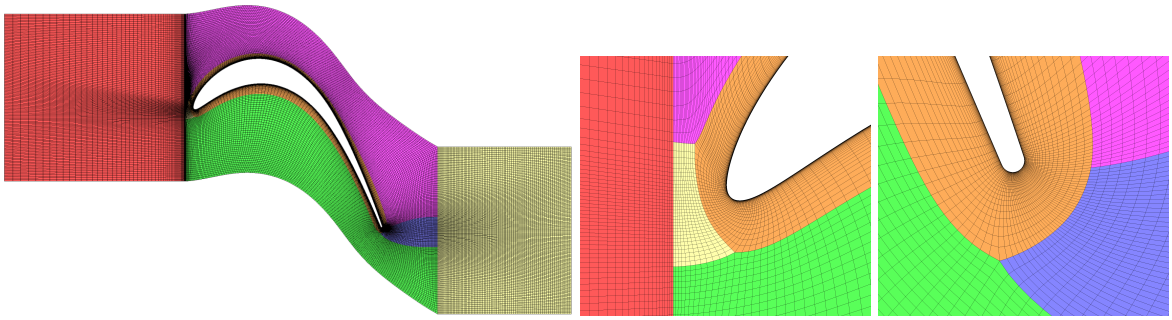

Figure 4: Channel grid with hexahedra elements

the mainstream air. All the walls (blade, cavity, upper and lower walls) are modelled with an adiabatic condition.

Finite volume *elsA* solver [15] has been used for the steady RANS simulations. The Roe upwind scheme [16] with a second order *van Albada* flux limiter [17] have been used. The time integration scheme is the implicit Euler method. The assessed turbulence models are the $k-l$ Smith, the $k-\omega$ SST Menter and the RSM SSG/LRR-ω.

The channel has been meshed following an "O-6H" structured topology (Fig. 4) created with Numeca AutoGrid software using hexahedral elements. The O-block allows to maximise the cells' orthogonality. The H-block upstream of the LE is very small. It has been limited by the presence of the upstream hub cavity. The minimum angle between two contiguous face of the cells (orthogonality) is 30°. For the same configuration, Fiore [18] has worked with a mesh of 30° minimum orthogonality. The fully hexahedra mesh constitutes the reference configuration without cavity.

For the configurations with a cavity, the same channel mesh is used, and to account for the cavity, tetrahedral elements were used in it, in the chute and nearby in the channel area. The use of tetrahedral elements offers more flexibility and allows local refinement without modifying the channel mesh. Figure 5 shows the grids in which the two parts are visible: the channel and

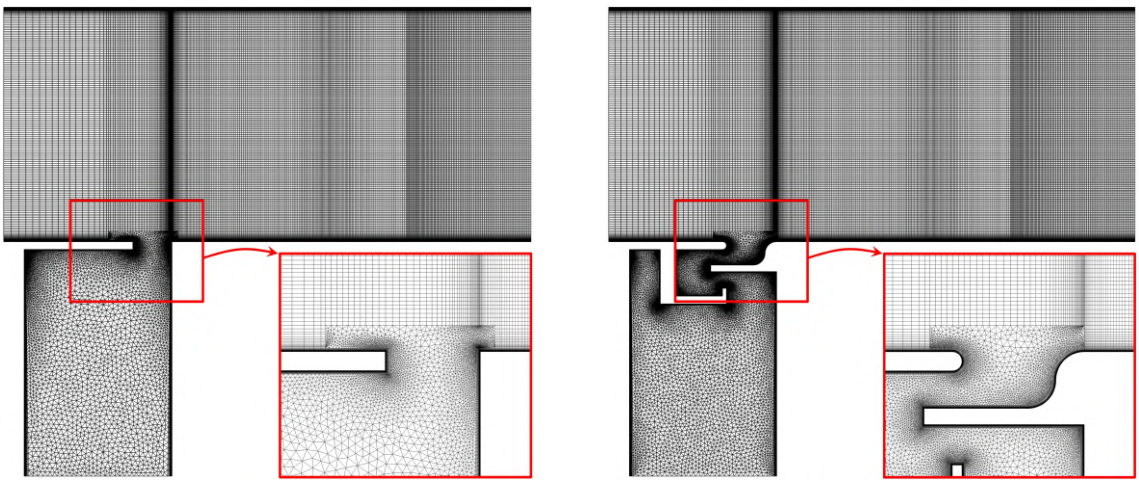

Figure 5: Hybrid mesh of the linear cascade with (a) axial and (b) compound cavity

the cavities. The wall cell size, y^+, is less than 0.6 in the whole computational domain, and the expansion ratio in the boundary layer is 1.15. The total number of cells is 8.5 millions in the channel, 3 millions inside the axial cavity, and 5 millions in the compound cavity.

RESULTS AND DISCUSSION

Modelling of external turbulence with RANS

The experimental configuration has a high external turbulence level which needs be modelled in the numerical simulations. The turbulence intensity measured upstream of the LE is 6%. A turbulent dissipation length (8 mm) consistent with the experimental turbulence grid is used in the simulations. For eddy-viscosity models, this leads to a large value of eddy viscosity (μ_t/μ=1150) at the inlet of the computational domain. Yet, such high values of eddy viscosity for Boussinesq models result in excessive turbulent diffusion increasing the mixing. Figure 6 shows that the $k-\omega$ SST model (Tu=6%) reduces the gradients of stagnation pressure losses (ζ) and overpredicts the losses by a factor of 2, while the SSG/LRR-ω model predicts losses close to the measurements. When the external turbulence rate is reduced (Tu=1%), the effect of the turbulent diffusion for the $k-\omega$ SST model is also decreased. Indeed the loss peaks predicted by the $k-\omega$ SST model (Tu=1%) at 30% and 70% channel height are less spread with reduced losses over the entire channel height. Only the SSG/LRR-ω model is able to accurately account for the high external turbulence level without altering the behaviour of the mean flow. Unlike Boussinesq models, which model a turbulent viscosity (μ_t) increasing the diffusion term in the RANS momentum equations, RSM models do not incorporate turbulent viscosity and instead model each Reynolds stress component separately.

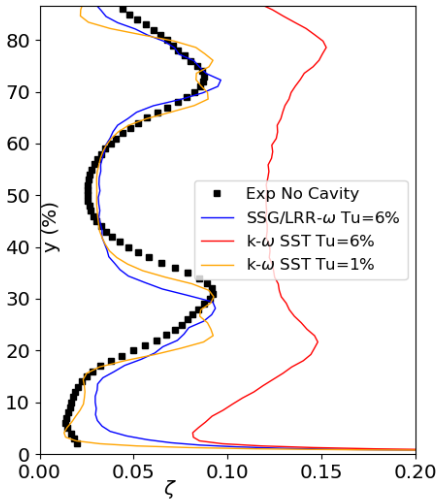

Figure 6: ζ radial profile

In a Boussinesq model, the decay of turbulence quantities is given by [19]:

$$\frac{k}{k_{\text{Freestream}}} = \left[1 + (C_{\varepsilon 2} - 1)\left(\frac{\varepsilon}{k}\right)_{\text{Freestream}} \frac{x}{U}\right]^{\frac{-1}{C_{\varepsilon 2}-1}} \tag{1a}$$

$$\frac{\nu_t}{\nu_{t,\text{Freestream}}} = \left[1 + (C_{\varepsilon 2} - 1)\left(\frac{\varepsilon}{k}\right)_{\text{Freestream}} \frac{x}{U}\right]^{\frac{C_{\varepsilon 2}-2}{C_{\varepsilon 2}-1}} \tag{1b}$$

with a constant U velocity, ε represents the turbulence dissipation, $\nu_t = \mu_t/\rho$, $C_{\varepsilon 2} = 1.92$. The decay of k is faster than that of ν_t (exponent in Eq.1a is -1.1 vs. -0.09 in Eq.1b). The high level of turbulent viscosity injected at the inlet of the domain persists throughout the computational domain due to this slow decay. It actively participates in the diffusion of the secondary structures, leading to increased aerodynamic losses as shown in Fig. 6.

Therefore, the external turbulence will be ignored in simulations with eddy-viscosity models ($k-l$ and $k-\omega$ SST) in the present work.[2] This simplification is not expected to change the major conclusions concerning the comparison between the models.

[2]The authors wish to indicate that slight anomalies were observed locally at the inlet and outlet (unexplained rise of $\sim$ 10 Pa) of the computational domain with the RSM model for large turbulence rate. Besides these numerical artefacts, that remain to be understood, the authors are confident with the numerical results with this model.

Flow topology

The purge flow has an essential role in sealing the cavity from the hot air. It also feeds vortex structures in the inter-blade region. Figure 7 shows the amplification of the near-hub passage vortex compared to near-shroud regions with isovalue surfaces of Q-criterion. The near-hub structure is larger than the one at the top of the blade which is far from the purge flow. The passage vortex is created at the LE and migrates towards the suction side of the neighbouring blade under the effect of the pressure gradient. The recirculation visible after the inner-cavity fin reduces the *vena contracta* and thus helps in sealing the cavity.

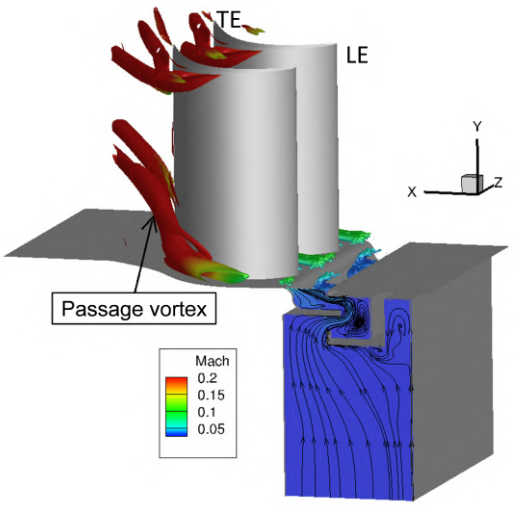

Figure 7: Q-criterion (SSG/LRR-ω)

Purge flow influence

The influence of the purge flow has been investigated through the variation of its mass flow in the axial configuration. The pressure losses at the exit of the cascade, the cavity sealing and the influence of the purge on the flow around the blade have been scrutinised. The stagnation pressure maps at 1/4 C_x downstream of the TE are gathered in Fig. 8. The losses appear in green and blue in areas that correlate with the wake of the blade and different vortex structures that develop in the channel inter-blade zone. Three distinct structure footprints are visible in the measurements, which are attributed to the wall (A), passage (B), and corner (C) vortices [4]. In the reference purgeless case, the passage vortex is the biggest among these structures. The

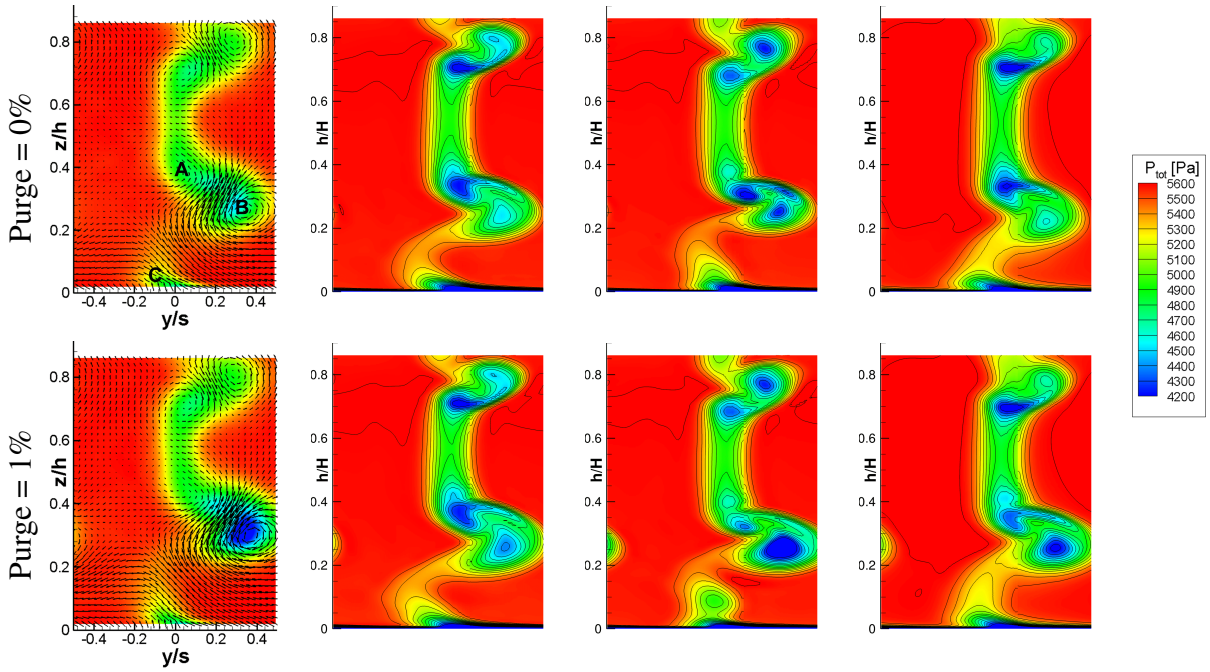

Exp. $k-l$ $k-\omega$ SST SSG/LRR-ω

Figure 8: Stagnation pressure (P_i-$P_{i,amb}$) map at 1/4 C_x downstream of the TE (axial chute)

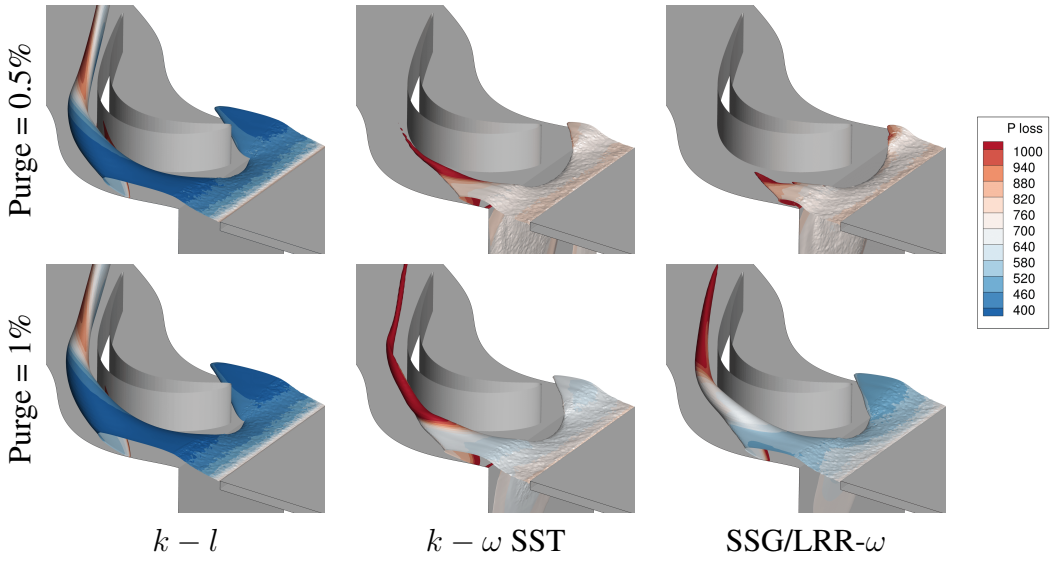

Figure 9: Iso-surface of stagnation temperature θ below mainstream temperature (θ = 0.85) colored by ($P_{i,inlet}$-P_i) (axial chute)

presence of the cavity amplifies this vortex, causing the footprint of the pressure losses in the lower part of the channel to be greater than the upper part. When a purge flow is injected (purge mass flow = 1%), this vortex is further amplified. Apart from the passage vortex, the rest of the flow seems to be undisturbed by the purge flow whose influence on the pressure field is limited to the lower 40% of the channel. The simulations with the three turbulence models show the same trend but with overestimating losses in the core of the vortices. The same behaviour is also shown by François and Gand [20] with a Spalart-Allmaras turbulence model. They also show that a hybrid RANS/LES simulation reduces significantly the overestimations.

It is worth noting that while the $k-l$ model predicts a slight increase in the passage vortex related loss, the two other models predict a footprint which is in better agreement with the measurements (Fig. 8). The purge flow feeds the passage vortex and due to its radial migration the losses are not confined near the hub. Figure 9 shows how the flow exiting the cavity contributes to the amplification of the passage vortex. An iso-surface of temperature $\theta = (T_i - T_{i,leakage})/(T_{i,\infty} - T_{i,leakage})$ reveals how far the penetration of the cooling purge flow disturbance in the channel goes ($\theta = 1$: channel flow temperature, and $\theta = 0$: cavity temperature). Due to the potential effect of the blade LE, the flow exits the chute periodically in the channel inter-blade area. Once out, the purge flow is mixed with the near-wall low velocity passage vortex which amplifies with the increasing purge. This structure is then pushed towards the suction side of the blade by the pressure differential. As opposed to the $k-\omega$ SST and SSG/LRR-ω models, the $k-l$ model predicts a contribution of the purge flow on the development of the passage vortex that is only slightly modified when the mass flow increases. The $k-\omega$ SST model predicts a thinner temperature isovalue surface but with a more intense pressure loss. This analysis must be verified by the level of mixing in the cavity. Indeed, the iso-surfaces presented in Fig. 9 are highly dependant on the cavity and chute temperature mixing.

To better understand the differences in the development of the passage vortex, an investigation of the flow near the chute exit is necessary. For that purpose, Fig. 10 shows the streamlines and the temperature mixing indicator, θ, at the cavity LE plane. The pressure potential effect

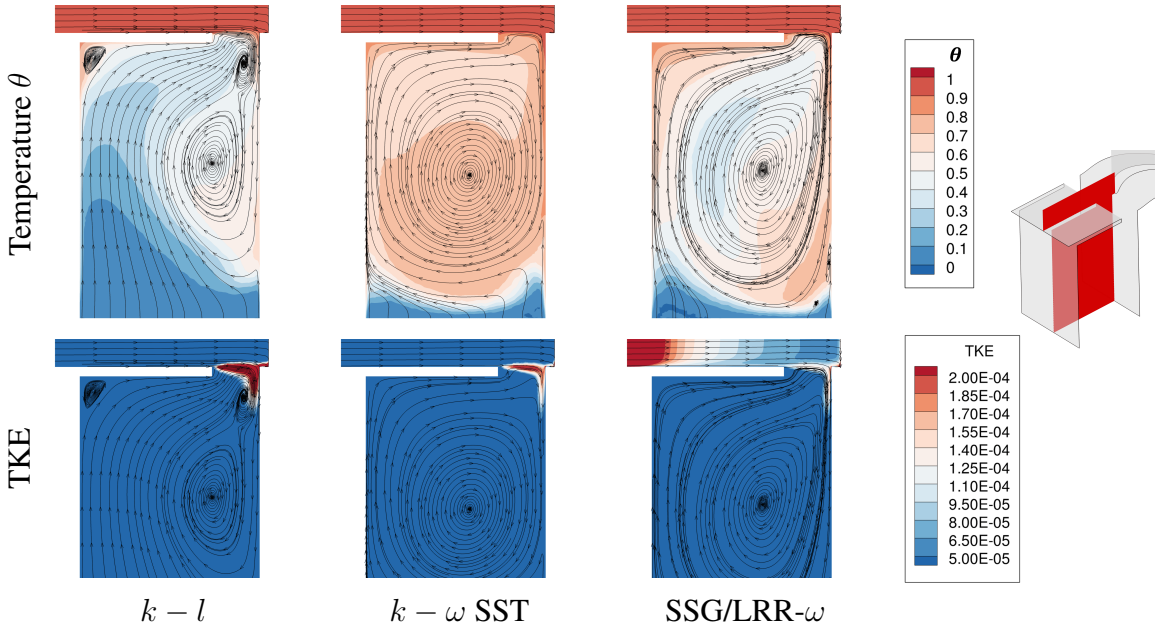

Figure 10: θ and normalised TKE in the LE plane of the cavity (axial chute, purge flow = 1%)

induces the ingress in the LE plane which is predicted by all of the models. However, the level of ingress seems to be higher for $k-\omega$ SST and SSG/LRR-ω where the hot air penetrates deeper and the temperature mixing occurs in the entire cavity, while this happens mainly in the near-chute area with the $k-l$ model. Therefore, the temperature isovalue surface in Fig. 9 is thicker for the $k-l$ model: the temperature mixing continues out of the cavity. One explanation of this phenomena lies in the recirculation that is present in the outlet of the chute (Fig. 10). This vortex structure limits the flow crossing the chute from the channel to the cavity. The creation of this vortex structure can be attributed to the production of turbulent kinetic energy in the shear layer at the intersection of the two flows. Uncu *et al.* [21] found a similar behaviour of overproduction of TKE for the $k-l$ model in a jet in crossflow. It is worth mentioning the inlet turbulence decay for the RSM model in the channel which is not visible for the two other models according to the modelling choice.

The purge flow also changes the mean angle of the flow coming to the blade. This angle modification disrupts the velocity triangle and the pressure distribution. The predictions of the pressure field, $C_p = {}^{(P_{i,1}-P_s(x))}/_{(P_{i,1}-P_{s,2})}$, around the blade in the near-hub region (6% channel height) are presented in Fig. 11. At the pressure side, with no purge flow, all the models predict a pressure distribution close to the experiment. At the suction side, they predict a decrease of pressure higher than the measurements from the mid-chord. The distribution of pressure is all the more discriminatory when purge flow is injected (Fig. 11-b). The ingress and egress topology are different between the $k-l$ model and the other simulations. As a consequence, the work on the blade is modified and different pressure distributions are noticeable from the LE on both sides. More precisely, a pressure decrease at the pressure side between $x/C_x = 0.2$ and $x/C_x = 0.5$ is visible with this model, and the pressure is also underestimated at the suction side from $x/C_x = 0.3$ which corresponds to the location where the purge-amplified passage vortex migrates towards the blade suction side. The SSG/LRR-ω model is the one that fits the measurements best, both on suction and pressure sides.

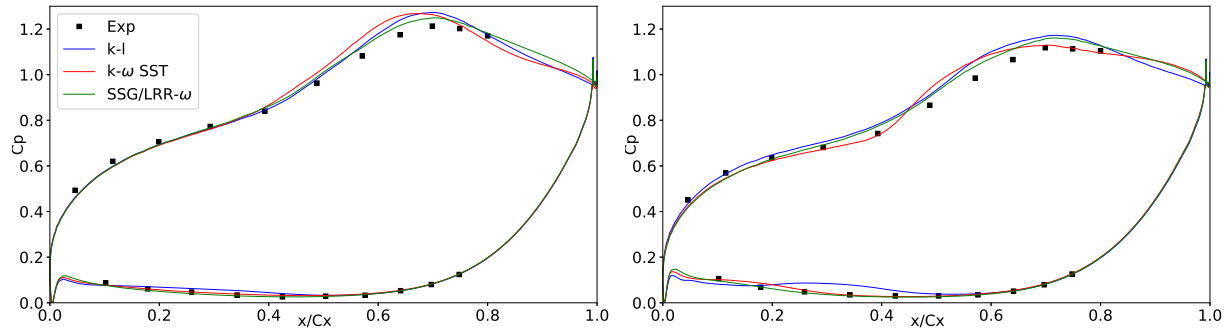

(a) (b)

Figure 11: C_p around the blade at 6% channel height for a purge mass flow of (a) 0% and (b) 1% (axial chute)

Cavity geometry influence

An increased purge flow improves the chute sealing at the expense of additional aerodynamic losses. A better sealing is possible by changing the chute geometry and maintaining the same purge mass flow. The simulation results from the two geometries presented in Fig. 2 are now compared. Figure 12 shows the ingress and egress on the LE and inter-blade planes. The temperature field shows that the level of ingress is very low for the compound geometry. Even at the LE plane, where the pressure potential field pushes mainstream flow into the cavity for the axial configuration, the recirculations created at the compound chute exit blocks the passage. The same phenomenon (recirculation inside the seal) deeper in the compound chute occurs in the inter-blade plane. The predictions of the structures for the compound case

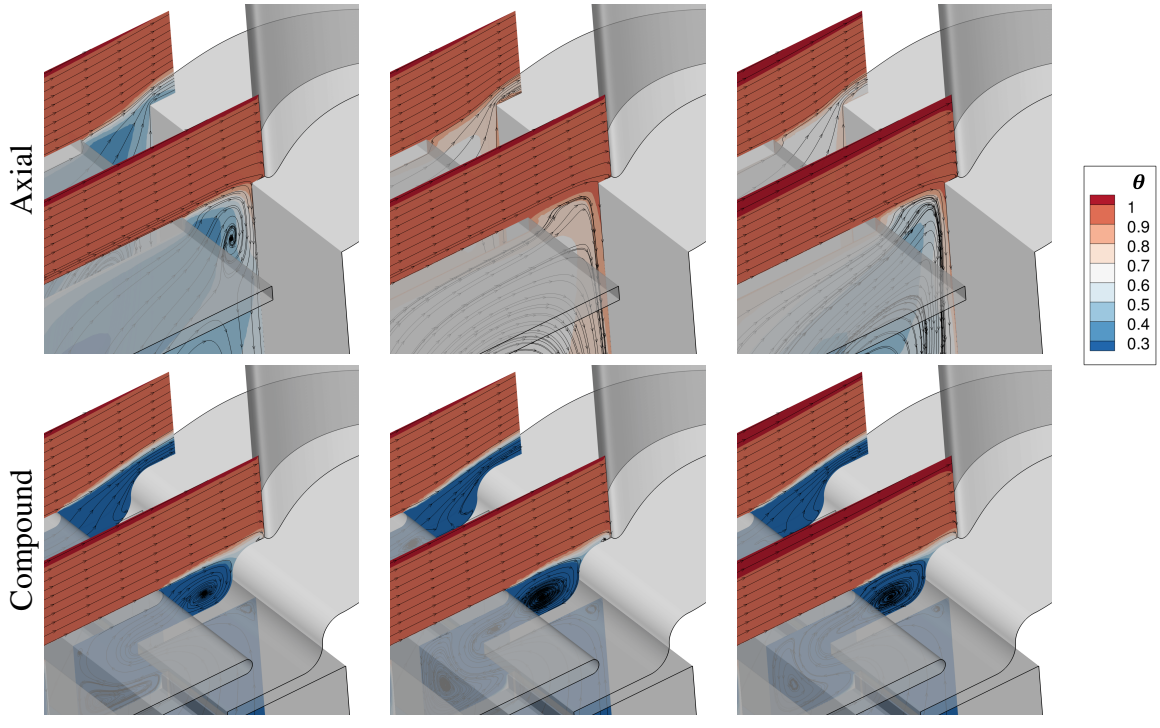

Figure 12: Streamlines and temperature, θ, in the cavity exit region (purge flow = 1%)

are very similar for the three models. The axial configuration, which does not have an inner fin, is exposed to the mainstream flow. Levels of ingress and egress are stronger. Another difference lies in the distance of radial penetration of the purge jet in the channel. Figure 13 shows that the smooth angle between the compound chute and the hub helps realign the streamlines in the direction of the mainstream flow, while for the axial case the penetration is deeper. The $k-\omega$ SST and SSG/LRR-ω models predict a recirculation downstream of the platform edge in the inter-blade plane of the axial cavity (Fig. 12). The ingress/egress map presented in Fig. 14 shows that the amplitude of flow entering the cavity is quite high in the axial case. The redirection at the compound chute exit decreases the effect of the potential field. Except the $k-l$ model, which shows less egress in the upstream part of the compound chute, the models predict the same quantities and regions where the flow is entering and exiting the compound chute. The main differences occur for the axial geometry as discussed in the precedent section. For the axial geometry, the $k-l$ model predicts an egress which is inferior to the two other models (Fig. 14). This is due to the lower ingress in the LE plane (Fig. 10) and the conservation of mass.

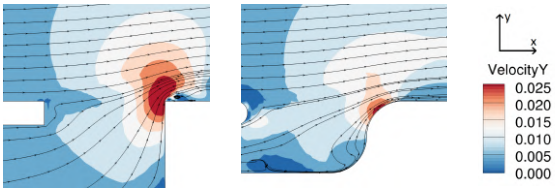

Figure 13: Streamlines at chute exit inter-blade area (purge flow = 1%, SSG/LRR-ω)

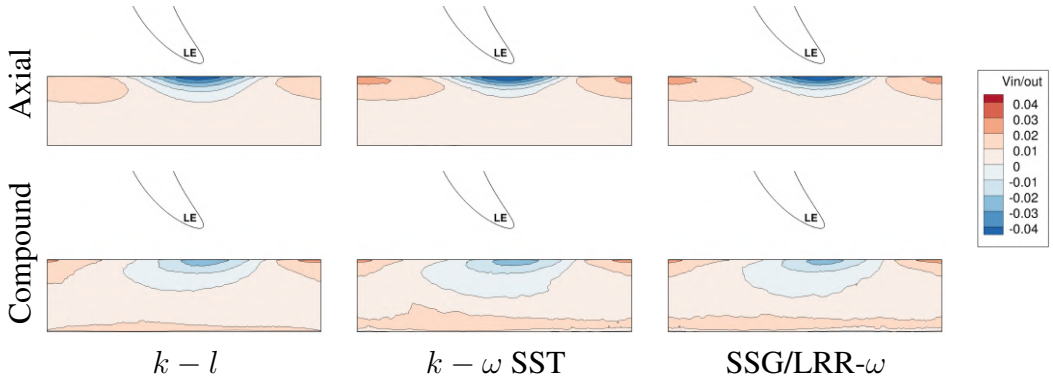

Figure 14: Cavity chute ingress (blue) / egress (red) (normalised normal velocity) upstream of the LE (purge mass flow = 1%)

The difference in the topology of the *jet* exiting the chute also modifies the secondary structures created in the inter-blade area. An increased size of the passage vortex is expected for the axial geometry according to the egress map. Consequently, the aerodynamic losses that are shown in Fig. 15, and defined as $\zeta = {(P_{i,1}-P_{i,2})}/{(P_{i,2}-P_{s,2})}$, are higher for the axial case. The peak at 30% height corresponds to the passage vortex (zone B in Fig. 8) and the peak at 40% to the wall vortex (zone A). These two vortices seems to be amplified when a cavity is present and when a purge flow is injected (Fig. 8). However, the difference between the two cavities in terms of aerodynamic losses lies only on the size of the passage vortex. The peak corresponding to the passage vortex radial location is bigger for the axial cavity. The cavity generates additional aerodynamic losses until 60% of channel height. Above, the channel remains undisturbed by the presence of the cavity. The $k-l$ model predicts aerodynamic losses that are very similar for both of the cavity shapes. Its sensitivity towards the chute geometry is absent. Indeed, the $k-l$ model does not predict an amplification of the passage vortex when an axial chute is

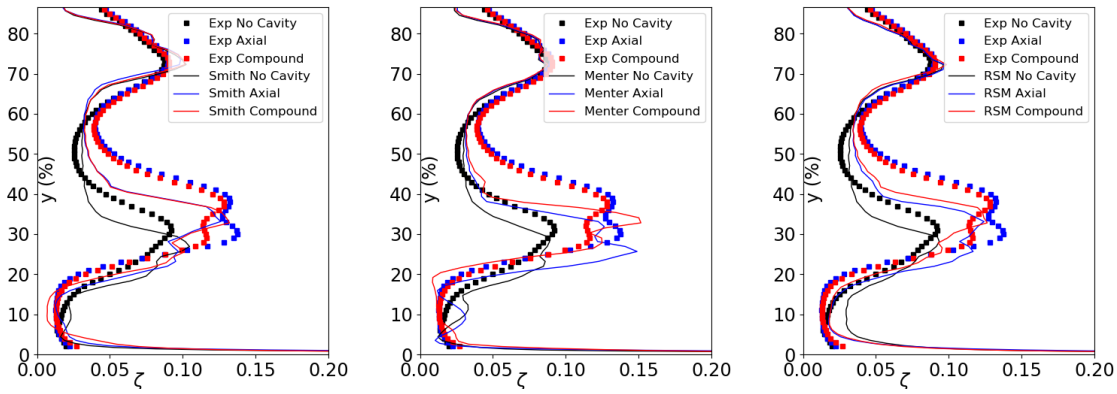

(a) $k-l$ (b) $k-\omega$ SST (c) SSG/LRR-ω

Figure 15: Radial profiles of ζ with the (a) $k-l$, (b) $k-\omega$ SST and (c) SSG/LRR-ω model for the configurations w/o, axial and compound cavities (purge flow = 1%)

simulated. The underestimation of axial geometry losses for this model can be attributed to the lower amplitude of the egress prediction. The $k-\omega$ SST model shows a noteworthy difference. The compound cavity reduces passage vortex footprint, while the wall vortex size increases. The amplified aerodynamic loss peaks are inversed compared to the measurements. Despite predicted losses that are slightly inferior to the measurements, only the SSG/LRR-ω model is able to reproduce an accurate evolution of the losses for the three configurations studied. The SSG/LRR-ω model predictions of the relative gap of pressure loss amplification between axial and compound chute are the same as in the measurements. Notice, however, that all of the three models cannot accurately predict the radial migration of the secondary structures. The simulated pressure loss peaks are closer to the hub than in the measurements.

CONCLUSIONS

Two cavity chute geometries and three purge mass flows have been simulated with three different RANS turbulence models: the SSG/LRR-ω, $k-l$ and $k-\omega$ SST. The high level of external turbulence in the configuration discriminates the two eddy-viscosity models which predict too much turbulent diffusion causing an overestimation of pressure losses. The external turbulence rate is accounted for only with the SSG/LRR-ω model. All the utilised models predict the increase in the passage vortex size when a cavity with purge is present. The main differences between the models appear at the exit of the axial chute where an extra vortex structure is predicted by the $k-l$ model, which modifies the ingress/egress topology. The pressure distribution around the blade predicted by the same model does not agree well with the measurements. Only the SSG/LRR-ω model is able to capture the difference of losses between an axial and compound cavity. While all the models show that the ingress is eliminated with the compound chute, the two eddy-viscosity models are not able to predict the benefit of this geometry in terms of aerodynamic losses. The non-linear RSM SSG/LRR-ω model seems to be better-suited for simulating purge/mainstream flow interactions. In the future, it would be worth assessing the SSG/LRR-ω model in a real turbine configuration where the flow is compressible and rotational stress is created by the rotating cavity chute walls.

ACKNOWLEDGEMENTS

The authors wish to thank Georges Gerolymos (Sorbonne University), and Jacques Demolis (Safran Helicopter Engines) for their help in the analysis of turbulence modelling impacts.

REFERENCES

[1] B. V. Johnson, G. J. Mack, R. E. Paolillo, and W. Daniels. *Turbine rim seal gas path flow ingestion mechanisms*. AIAA Reston, VA, USA, 1994.

[2] F. J. Bayley and J. M. Owen. The Fluid Dynamics of a Shrouded Disk System With a Radial Outflow of Coolant. *Journal of Engineering for Power*, 92(3):335–341, 07 1970.

[3] S. S. Savov, N. R. Atkins, and S. Uchida. Comparison of Single and Double Lip Rim Seal Geometry. volume 5A: Heat Transfer of *Turbo Expo: Power for Land, Sea, and Air*, 06 2016.

[4] P. Schuler, K. Dullenkopf, and H.-J. Bauer. Investigation of the Influence of Different Rim Seal Geometries in a Low-Pressure Turbine. volume 7: Turbomachinery, Parts A, B, and C of *Turbo Expo: Power for Land, Sea, and Air*, pages 715–729, 06 2011.

[5] T. Kluge, L. Wein, R. Schmierer, and J. R. Seume. Sensitivity analysis, design, instrumentation, and experimental validation of a novel labyrinth seal rig. *Proc ETC 13', European Turbomachinery Society*, 2019.

[6] R. R. Jones, O. J. Pountney, B. L. Cleton, L. E. Wood, B. D. J. Schreiner, A. J. C. Figueiredo, J. A. Scobie, D. J. Cleaver, G. D. Lock, and C. M. Sangan. An Advanced Single-Stage Turbine Facility for Investigating Non-Axisymmetric Contoured Endwalls in the Presence of Purge Flow. volume 2B: Turbomachinery of *Turbo Expo: Power for Land, Sea, and Air*, 06 2019.

[7] R. Da Soghe, C. Bianchini, M. Micio, J. D'Errico, and F. Bavassano. Effect of Rim Seal Configuration on Gas Turbine Cavity Sealing in Both Design and Off-Design Conditions. volume 5B: Heat Transfer of *Turbo Expo: Power for Land, Sea, and Air*, 06 2018.

[8] J. T. M. Horwood, F. P. Hualca, M. Wilson, J. A. Scobie, C. M. Sangan, G. D. Lock, J. Dahlqvist, and J. Fridh. Flow Instabilities in Gas Turbine Chute Seals. *Journal of Engineering for Gas Turbines and Power*, 142(2), 01 2020.

[9] J. T. M. Horwood, F. P. Hualca, M. Wilson, J. A. Scobie, C. M. Sangan, and G. D. Lock. Unsteady Computation of Ingress Through Turbine Rim Seals. volume 5B: Heat Transfer of *Turbo Expo: Power for Land, Sea, and Air*, 06 2018.

[10] M. G. Izenson, M. R. Kennedy, and J. R. Sirukudi. Turbulent Flow Computations for Turbine Disk Cavity Flows. volume 1: Turbomachinery of *Turbo Expo: Power for Land, Sea, and Air*, 06 1995.

[11] L. Porreca, M. Hollenstein, A. I. Kalfas, and R. S. Abhari. Turbulence measurements and analysis in a multistage axial turbine. *Journal of Propulsion and Power*, 23(1):227–234, 2007.

[12] R.-D. Cécora, R. Radespiel, B. Eisfeld, and A. Probst. Differential reynolds-stress modeling for aeronautics. *AIAA Journal*, 53(3):739–755, 2015.

[13] F. R. Menter. Two-equation eddy-viscosity turbulence models for engineering applications. *AIAA Journal*, 32(8):1598–1605, Aug. 1994.

[14] B. Smith. A near wall model for the k-l two equation turbulence model. In *Fluid Dynamics Conference*, page 2386, 1994.

[15] L. Cambier, S. Heib, and S. Plot. The Onera elsA CFD Software: Input from Research and Feedback from Industry. *Mechanics & Industry*, 14(3):159–174, 2013.

[16] P. Roe. Approximate Riemann Solvers, Parameter Vectors, and Difference Schemes. *Journal of Computational Physics*, 43(2):357–372, 1981.

[17] G. van Albada, B. van Leer, and Roberts. A Comparative Study of Computational Methods in Cosmic Gas Dynamics. *Astronomy and Astrophysics*, 108:76–84, 04 1982.

[18] M. Fiore. *Influence des Ecoulements de Cavité Inter-disque sur l'Aérodynamique d'une Turbine*. PhD thesis, Université de Toulouse, 2019.

[19] P. R. Spalart and C. L. Rumsey. Effective Inflow Conditions for Turbulence Models in Aerodynamic Calculations. *AIAA journal*, 45(10):2544–2553, 2007.

[20] B. François and F. Gand. Hybrid RANS/LES Simulations of Secondary Flows in a Linear Cascade of Turbine Blades with External Turbulence. In *15th European Conference on Turbomachinery Fluid dynamics & Thermodynamics*, 2023.

[21] F. Uncu, B. François, N. Buffaz, and S. Le Guyader. Assessment of RANS Turbulence Models on Simplified Geometries Representative of Turbine Blade Tip Shroud Flow. volume 10B: Turbomachinery of *Turbo Expo: Power for Land, Sea, and Air*, 06 2022.